Activation of Peracetic Acid with $CuFe_2O_4$ for Rhodamine B Degradation: Activation by Cu and the Contribution of Acetylperoxyl Radicals

Chengzhi Yu [1], Libin Zheng [1], Yongyuan Hong [1], Jiabin Chen [1], Feng Gao [1,*], Yalei Zhang [1,2], Xuefei Zhou [1,2] and Libin Yang [1,*]

1   State Key Laboratory of Pollution Control and Resource Reuse, College of Environmental Science and Engineering, Tongji University, Shanghai 200092, China
2   Shanghai Institute of Pollution Control and Ecological Security, Tongji University, Shanghai 200092, China
*   Correspondence: gaofeng_1111@126.com (F.G.); neuqyanglibin@126.com (L.Y.)

Abstract: Advanced oxidation processes (AOPs) demonstrate great micropollutant degradation efficiency. In this study, $CuFe_2O_4$ was successfully used to activate peracetic acid (PAA) to remove Rhodamine B. Acetyl(per)oxyl radicals were the dominant species in this novel system. The addition of 2,4-hexadiene (2,4-HD) and Methanol (MeOH) significantly inhibited the degradation efficiency of Rhodamine B. The $\equiv Cu^{2+}/\equiv Cu^+$ redox cycle dominated PAA activation, thereby producing organic radicals (R-O·) including $CH_3C(O)O$· and $CH_3C(O)OO$·, which accounted for the degradation of Rhodamine B. Increasing either the concentration of $CuFe_2O_4$ (0–100 mg/L) or PAA (10–100 mg/L) promoted the removal efficiency of this potent system. In addition, weakly acid to weakly alkali pH conditions (6–8) were suitable for pollutant removal. The addition of Humid acid (HA), HCO_3^-, and a small amount of Cl^- (10–100 $mmol \cdot L^{-1}$) slightly inhibited the degradation of Rhodamine B. However, degradation was accelerated by the inclusion of high concentrations (200 $mmol \cdot L^{-1}$) of Cl^-. After four iterations of catalyst recycling, the degradation efficiency remained stable and no additional functional group characteristic peaks were observed. Taking into consideration the reaction conditions, interfering substances, system stability, and pollutant-removal efficiency, the $CuFe_2O_4$/PAA system demonstrated great potential for the degradation of Rhodamine B.

Keywords: peracetic acid (PAA); rhodamine B; copper ferrite ($CuFe_2O_4$); organic radicals (R-O·)
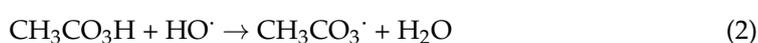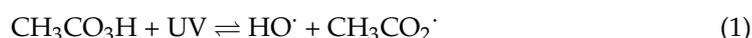
1. Introduction

With the increasing maturity of activated sludge processing technologies and physico-chemical treatment methodologies, common pollutants present in sewage represented by parameters such as the chemical oxygen demand (COD), nitrogen content, and phosphorus content have been effectively treated. However, there are still problems associated with the removal of micropollutants with complex structures, which has spurred great research interest in recent years. Due to the appreciable removal performance of persistent organic pollutants in sewage effluent and industrial wastewater, advanced oxidation processes (AOPs) have attracted more and more attention and have been considered one of the most promising technical treatment options [1–3]. AOPs consist of various technologies, such as ozonation, photocatalytic oxidation, Fenton-like oxidation, electrochemical oxidation, etc. The basis for these treatment methodologies relies on reactive oxygen species (ROS) such as hydroxyl radicals, sulfate radicals, and organic radicals [4–6].

Several oxidants such as hydrogen peroxide (H_2O_2), ozone (O_3), persulfate (PDS), and peroxymonosulfate (PMS) are used in AOPs to generate free radicals [7–9]. Hydrogen peroxide is the most-used oxidant because of the high activity of its oxidizing species (e.g., HO·). Moreover, these oxidizing species are capable of completely and non-selectively destroying recalcitrant organic contaminants [10]. Recently, the application of peracetic

acid (PAA) in AOPs has been studied. PAA, a peroxy acid oxidant, has been widely used for disinfection and sterilization in textile industries, aquaculture, medical applications, and food processing [11,12]. Owing to its low toxicity, less harmful byproducts, and high disinfection efficiency, the application of PAA has increased continuously as an alternative disinfectant in wastewater treatment systems in Europe and North America. The standard reduction potential of PAA (relative to the standard hydrogen electrode) is 1.06–1.96 V, which is close to that of H_2O_2 (E_0 = 1.8 V) [11]. However, the peroxide bond energy of PAA is 159 kJ/mol, which is lower than that of hydrogen peroxide (HP, 213 kJ/mol) and PMS (317 kJ/mol) [13,14], indicating that PAA can be activated more easily to produce oxidative radicals. Moreover, PAA has less dependence on pH, and its decomposition products are non-toxic, safe, and biodegradable [15–19]. When integrated with biotreatment, these decomposition products can supply additional carbon sources [20]. In summary, PAA is an ideal novel oxidant; however, developing an efficient and pollution-free activation method of PAA is of great significance.

Many researchers have devoted significant time to exploring efficient catalysts for PAA activation, and considerable progress has been made on this front. In AOPs with PAA as the oxidant, degradation of persistent organic pollutants is driven by various radicals, including $OH^\cdot$ and $R\text{-}C^\cdot$ (e.g., $CH_3^\cdot$, $CH_3O_2^\cdot$, $CH_3CO^\cdot$, $CH_3CO_2^\cdot$, and $CH_3CO_3^\cdot$) [21,22]. Thus, the catalytic decomposition of PAA is more complicated compared with the activation of inorganic peroxides. Transition metals, ultraviolet/solar light irradiation, ultrasound, heat, electrochemical processes, and carbon catalysts are all techniques used in AOPs [22–24]. The techniques that have been most applied for PAA catalysis are UV radiation and the inclusion of transition metals. The dominant radicals may be different when different activation systems are applied. In the UV/PAA system, $HO^\cdot$ and $CH_3CO_2^\cdot$ are the initial products (Equation (1)). Subsequently, $CH_3CO_3^\cdot$ is generated (Equation (2)) [25].

$$CH_3CO_3H + UV \rightleftharpoons HO^\cdot + CH_3CO_2^\cdot \tag{1}$$

$$CH_3CO_3H + HO^\cdot \rightarrow CH_3CO_3^\cdot + H_2O \tag{2}$$

As for the transition metal/PAA system, the products are much more complex (Equations (3)–(8)), among which $CH_3CO_2^\cdot$ and $CH_3CO_3^\cdot$ are regarded as the dominant radicals, while little to no $HO^\cdot$ is generated [26,27].

$$CH_3C(O)OOH + M^{n+} \rightarrow M^{(n+1)+} + HO^- + CH_3COO^\cdot \tag{3}$$

$$CH_3C(O)OOH + M^{(n+1)+} \rightarrow M^{n+} + H^+ + CH_3COOO^\cdot \tag{4}$$

$$CH_3C(O)OOH \xrightarrow{M^{n+}} CH_3C(O)O. + HO. \tag{5}$$

$$CH_3C(O)OOH + HO^\cdot \rightarrow CH_3C(O)OO^\cdot + H_2O \tag{6}$$

$$CH_3C(O)O^\cdot \rightarrow CH_3^\cdot + CO_2 \tag{7}$$

$$CH_3^\cdot + O_2 \rightarrow CH_3O_2^\cdot \tag{8}$$
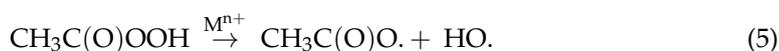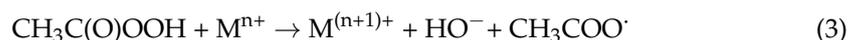
The different relative species that contributed to contaminant degradation were further probed in some studies. For example, it has been reported that $CH_3CO_2^\cdot$ and $CH_3CO_3^\cdot$ demonstrated a good organic compound removal efficiency for compounds such as naproxen, naphthyl compounds, phenol, 2-naphthoxyacetic acid, aniline, bezafibrate, acid orange 7, bisphenol-A, carbamazepine, diclofenac, ibuprofen, clofibric acid, methylene blue, sulfa drugs, and sulfamethoxazole. Furthermore, these radicals had a longer half-life than $HO^\cdot$ [28,29]. Zhou et al. [16] reported that in the PAA/activated carbon fiber system for the degradation of red X-3B, $HO^\cdot$ was not important compared to acetyl(per)oxyl radicals. Kim et al. [17] delineated that in the biphasic kinetics of Fe(II)/PAA contaminant degradation, acetyl(per)oxyl radicals, $HO^\cdot$, and Fe(IV) were responsible reactive species for the degradation of contaminants.

Transition metal/PAA systems may demonstrate greater promise in the future. However, toxicity and poor reusability bring hindrances to the application of transition metals in homogeneous processes [30]. To overcome these shortcomings, heterogeneous catalysis could be a good alternative. Yu et al. [31] successfully applied fabricated magnetically separable TiO_2-FeO_x-polyoxotungstate (POM) to 2,4-DCP degradation, which exhibited excellent performance. Karbasi et al. [32] studied the use of magnetized photocatalysts (Bi_2WO_6-FeO_x) to avoid the high separation cost of catalyst recycling. An environmentally benign and non-toxic catalyst for PAA activation is desirable based on sustainable and green development.

Recently, spinel-type particles with the general formula MFe_2O_4 (M = Cu, Zn, Co, Mn, etc.) have attracted great interest [33]. Spinel ferrite, a typical spinel ferrite, has a relatively stable structure, which reduces the leaching of heavy metals [34]. Another advantage of spinel ferrite is its magnetic property; thus, it can be easily separated from water for recovery [35]. Moreover, the spinel oxide powders could provide a larger surface area to assist the diffusion of reactants onto the active sites. Although $CoFe_2O_4$ has a better catalytic ability than $CuFe_2O_4$, the release of Co during the reaction may bring more risk of toxicity and carcinogenicity [36]. In recent studies, the PMS/$CuFe_2O_4$ system has been explored for the degradation of bisphenol-A at neutral pH values [37], and $CuFe_2O_4$ has been used to generate $SO_4^{\cdot}$ from PMS [38].

As a synthetic xanthene dye, Rhodamine B was often chosen as a target containment to investigate various AOPs systems [39–41]. In the present work, the degradation of Rhodamine B by peracetic acid activated with a spinel copper ferrite ($CuFe_2O_4$) was studied. The morphology, elemental composition, total pore volume, and BET surface area of the catalyst were systematically investigated. The influence of different pH conditions, PAA, and catalyst loading on the pollutant removal efficiency was explored. Furthermore, the activation mechanism and reactive species were further proposed. Finally, the effect of water matrices, reusability, and stability of the catalyst was discussed to see if the PAA/$CuFe_2O_4$ demonstrated a practical utilization value.

2. Results and Discussion

2.1. Characterization of the Catalyst

To understand the microstructure of the commercial catalyst, the surface morphology of $CuFe_2O_4$ was studied via SEM. As shown in Figure 1a, $CuFe_2O_4$ possessed a relatively regular shaped particle morphology. All catalysts contained small particles with even surfaces. The particles agglomerated together due to the magnetic properties of the material, which was consistent with previous findings. Furthermore, the elemental compositional analyses of the catalysts were conducted by Energy Dispersive X-ray Spectroscopy (EDS). As shown in Figure 1b, five elements were present in the commercial sample: O, Al, P, Fe, and Cu. The atomic contents of these elements were 69.5%, 1.46%, 6.05%, 16.39%, and 7.05%, respectively. The total pore volume of $CuFe_2O_4$ was 0.067 cm^3/g, and the BET surface area of $CuFe_2O_4$ was 19.4 m^2/g.

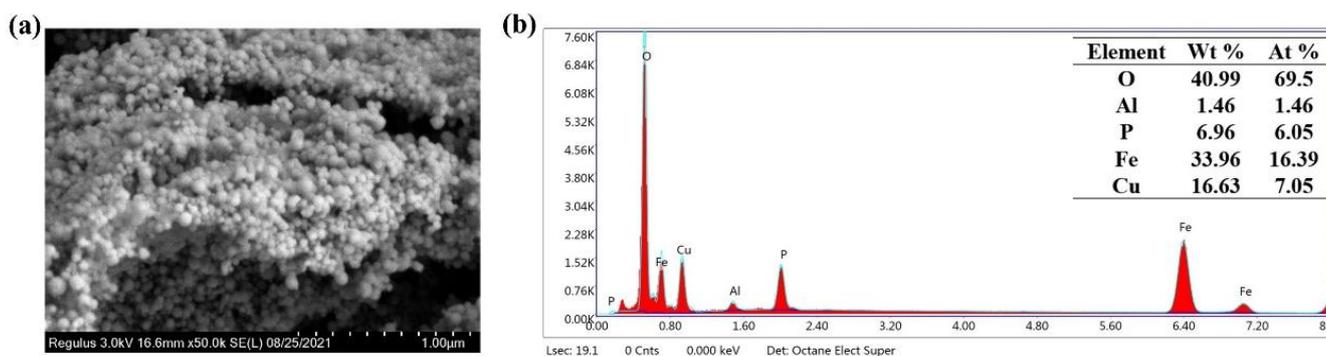| Element	Wt %	At %
O	40.99	69.5
Al	1.46	1.46
P	6.96	6.05
Fe	33.96	16.39
Cu	16.63	7.05

Figure 1. SEM image (**a**) and EDS spectroscopy (**b**) of $CuFe_2O_4$.

2.2. The Effect of Initial pH on Contaminant Degradation

In metal-based catalysis, the solution pH could affect the oxidation potential of a process, which is considered a crucial parameter for chemical oxidation reactions. The effect of initial pH on the degradation of Rhodamine B in the $CuFe_2O_4$/PAA system was further evaluated, as shown in Figure 2. Different degradation efficiencies could be observed at different pH values. At pH 4 and 9, the removal efficiencies of the system were 18.5% and 21.2% within 30 min, respectively. The sequence of degradation efficiencies under other selected pH values was as follows: pH 5 (47.9%) < pH 7 (66.4%) < pH 6 (72.8%) < pH 8 (77.5%). After 60 min of reaction, the sequence of degradation efficiencies changed to the following: pH 9 (41.4%) < pH 4 (43.6%) < pH 5 (84.3%) < pH 7 (91.4%) < pH 8 (94.4%) < pH 6 (95.4%). It can be inferred that the specific pH range (weakly acid to weakly alkaline conditions, including neutral conditions) was favorable for Rhodamine B decomposition. When the pH condition was higher than eight or lower than six, the removal efficiency decreased sharply. There were two possible causes for this phenomenon: the first was the abnormal decomposition of PAA and the second was the change of the catalyst state. For acidic conditions, it has been reported that the structure of PAA could remain stable under pH 3–5 [1]. In addition, PAA activation by Cu^{2+} could be suppressed under acidic conditions in AOP systems because high concentrations of H^+ could inhibit the generation of $CH_3CO_3^{\cdot}$ via Equation (9). Therefore, the degradation of Rhodamine B would be suppressed. Conversely, the causes changed for alkaline conditions. It has been reported in previous studies that the pKa of PAA was 8.2 [42], indicating that the self-decomposition of PAA can easily occur to produce $CH_3CO_3^-$ when the pH was 9 or greater. Moreover, PAA was a precursor for H_2O_2 according to Equation (10) [43]. Therefore, the generation of $CH_3CO_3^-$ and the reaction between H_2O_2 and $CH_3CO_3^-$ via Equation (11) caused the reduction of PAA, which affected the generation of radicals due to the lack of substrate activation. In terms of the catalyst, the high OH^- concentration could also suppress the generation of radicals via Equation (12). Moreover, the $Cu(OH)_2$ complex formed under alkaline conditions through the reaction between $CuFe_2O_4$ and OH^- [1], which had a lower solubility and lower activity than free ions. In heterogeneous systems, these complexes are attached to the catalyst surface easily [44]. Therefore, the PAA activation efficiency was reduced by the reduction of both the catalyst and the contact area. In summary, the results showed that weakly acidic to weakly alkaline pH conditions were all suitable for PAA degradation in the $CuFe_2O_4$/PAA system. For actual sewage treatment (e.g., domestic sewage, livestock and poultry breeding wastewater, and some kinds of industrial wastewater), the $CuFe_2O_4$/PAA system holds practical value, without the need for excess acid and alkaline conditions.

$$Cu^{3+} + CH_3C(O)OOH \rightleftharpoons Cu^{2+} + CH_3C(O)OO^{\cdot} + H^+ \tag{9}$$

$$CH_3C(O)OO\,H + H_2O \rightleftharpoons H_2O_2 + CH_3C(O)OH \tag{10}$$

$$CH_3C(O)OO^- + H_2O_2 \rightarrow CH_3C(O)OO^- + H_2O + O_2 \tag{11}$$

$$CH_3C(O)OO\,H + Cu^{2+} \rightarrow Cu^{3+} + OH^- + CH_3C(O)O^{\cdot} \tag{12}$$

2.3. The Effect of PAA and Catalyst Loading on Contaminant Degradation

The degradation of Rhodamine B under different PAA concentrations and catalyst loadings in the $CuFe_2O_4$/PAA system at pH 7 was explored as summarized in Figure 3.

Figure 3a shows that the degradation of Rhodamine B was significantly enhanced, as the PAA concentration increased when 100 mg/L $CuFe_2O_4$ was added. When the PAA concentration increased from 10 mg/L to 100 mg/L, the degradation of Rhodamine B in the $CuFe_2O_4$/PAA system after 60 min increased from 40.9% to 99.0%. The results indicated that a higher PAA concentration produced more active radicals at the same time interval, which could accelerate the degradation of Rhodamine B. When the PAA concentration was 60 mg/L, the degradation efficiency of Rhodamine B after 60 min was 97.0%, while

a higher degradation efficiency (98.1%) was achieved in a shorter time (45 min) when the PAA concentration was 100 mg/L, which also supported the aforementioned finding. However, the removal efficiency reached 95.8% after 60 min when the PAA concentration was 80 mg/L; thus, further increasing the PAA loading was not conducive to controlling cost. In addition, negligible degradation of Rhodamine B was observed in the absence of PAA, illustrating that the adsorption of Rhodamine B by $CuFe_2O_4$ could be ignored (Figure S1).
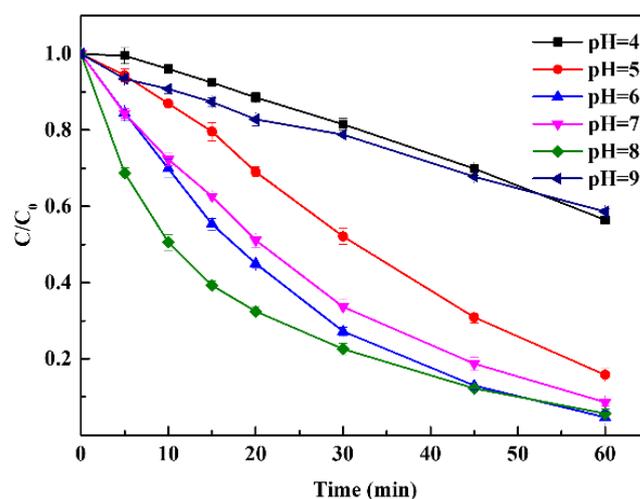

Figure 2. Effect of pH on Rhodamine B degradation ($CuFe_2O_4$ = 100 mg/L, PAA = 40 mg/L, C_0 = 20 mg/L, room temperature for 1 h).

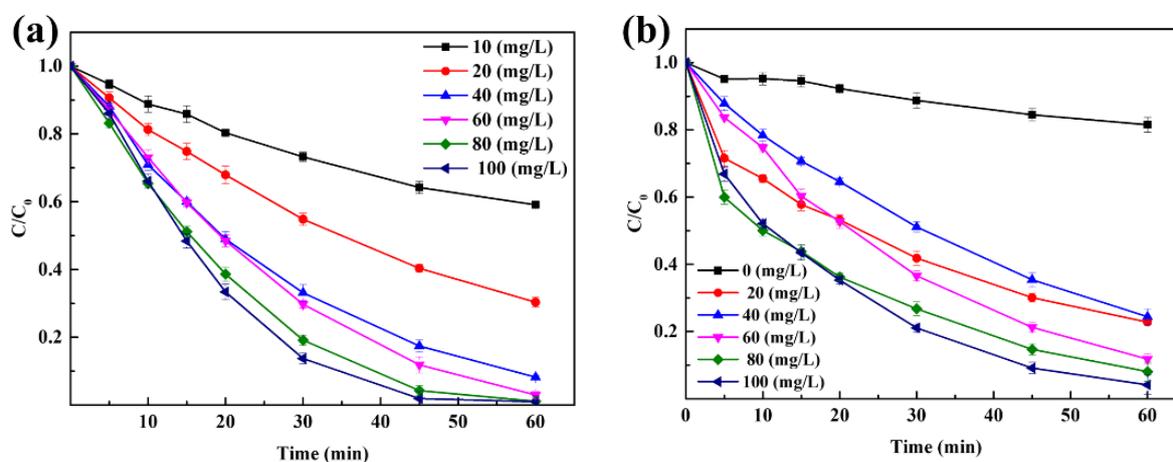**Figure 3.** (**a**) Effect of PAA loading on Rhodamine B degradation ($CuFe_2O_4$ = 100 mg/L, pH = 7, C_0 = 20 mg/L, room temperature for 1 h). (**b**) Effect of catalyst loading on Rhodamine B degradation (PAA = 80 mg/L, pH = 7, C_0 = 20 mg/L, room temperature for 1 h).

Figure 3b demonstrates that the degradation of Rhodamine B was significantly enhanced as the $CuFe_2O_4$ concentration increased when 80 mg/L PAA was added. In the absence of $CuFe_2O_4$, only 18.5% of Rhodamine B was degraded after 60 min, which indicated that the degradation of pollutants mainly depended on the presence of active species, and the oxidative degradation effect by PAA alone was relatively poor. When the $CuFe_2O_4$ concentration increased to 100 mg/L, the degradation of Rhodamine B in the $CuFe_2O_4$/PAA system after 60 min increased to 95.8%. The results showed that an increase in the $CuFe_2O_4$ concentration could provide ample active sites for PAA to generate more free radicals during the same time interval. In addition, as a kind of magnetic material, $CuFe_2O_4$ could be successfully separated by an external magnetic field. Therefore,

a higher catalyst loading was acceptable even if cost control was taken into consideration. This also suggested that $CuFe_2O_4$ had broader application prospects than other reported heterogeneous metallic catalysts for the treatment of aquatic micro-organic pollutants.

2.4. Identification of Activation Metal

The XPS spectra of Cu, Fe, and O in the $CuFe_2O_4$/PAA system before and after Rhodamine B degradation were obtained to illustrate the catalytic mechanism. The full-scale XPS spectrum of $CuFe_2O_4$ (the binding energies were corrected by the C 1s peak) is shown in Figure S2, which demonstrated the presence of Cu, Fe, and O. Other details are presented in Figure 4.
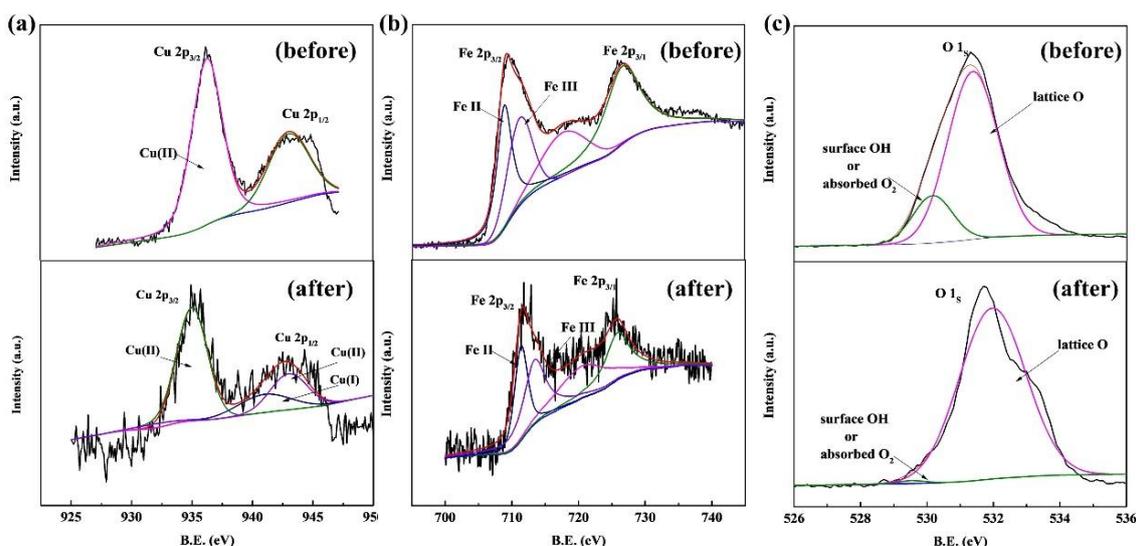

Figure 4. XPS spectra of $CuFe_2O_4$. (**a**) Cu. (**b**) Fe. (**c**) O.

Figure 4a shows the XPS spectrum of Cu 2p before and after the reaction. The binding energy peaks at 942.70 eV and 935.30 eV could be ascribed to Cu (II). After the reaction, the two peaks shifted to 943.98 eV and 935.57 eV, respectively. A new peak at 940.97 eV was observed after the reaction, suggesting the appearance of a new valence state which could be ascribed to Cu (I) [45]. The generation of Cu (I) illustrated that Cu (II) was reduced to a +1 valence state via the catalytic process, which was similar to PMS activation and could be explained by the coexisting oxidation and reduction processes (Cu^{2+}-Cu^+-Cu^{2+}) [14]. Figure 4b shows the XPS spectrum of Fe 2p before and after the reaction. The binding energy at 718.97 eV and 725.75 eV can be assigned to Fe^{2+} and Fe^{3+}, respectively [46]. Obviously, little to no redox reactions involving Fe^{2+}/Fe^{3+} occurred on the $CuFe_2O_4$ surface, which was deduced because the Fe valence state hardly changed, as indicated by the Fe $2p_{3/2}$ and Fe $2p_{1/2}$ sites after the reaction. Similar results were also reported in previous studies [29,47]. Although PAA activation has been reported in homogeneous systems via the Fe^{2+}/Fe^{3+} redox cycle, iron ions exhibited lower activity than copper ions. In heterogeneous systems, the contribution of the Fe^{2+}/Fe^{3+} redox cycle was limited to the catalyst surface at neutral pH conditions [29]. The O 1s XPS spectrum shown in Figure 4c illustrates two major peaks at 530.38 eV and 531.54 eV before the reaction. These peaks were assigned to the lattice O and surface adsorbed oxygen (or surface hydroxyl species), respectively [48,49]. The proportions of lattice O and adsorbed oxygen (or surface hydroxyl species) before the reaction were 6.7% and 93.3%, respectively, while lattice O nearly disappeared after the reaction. It can be inferred that strong hydroxylation reactions happened on the catalyst surface during the oxidation process. The decrease of lattice oxygen was due to the reduction of Cu^{2+} to Cu^+, and the increase of surface hydroxyl species could be attributed to the formation of Cu-OH complexes via Equations (13) and (14).

2.5. Identification of Reactive Species

Several organic radicals (e.g., $CH_3COO^{\cdot}$, $CH_3COOO^{\cdot}$, $CH_3^{\cdot}$, and $CH_3CO_2^{\cdot}$) and $OH^{\cdot}$ have been reported in PAA activation AOP systems. To identify the free radicals that played a major role in the process, three kinds of radical scavengers (MeOH, PBA, and 2,4-hexadiene (2,4-HD)) were tested in the $CuFe_2O_4$/PAA processing system, as shown in Figure 5. TBA is a widely used $OH^{\cdot}$ quencher with a second order rate constant of 3.8–7.6×10^8 but zero-order with respect to acetyl(per)oxyl radicals [50]. When 100 mmol·L^{-1} TBA was added into the $CuFe_2O_4$/PAA system, the degradation of Rhodamine B was not impacted to a great extent. The final removal efficiency was 98.6% after 60 min of reaction, demonstrating a small difference from the condition with no TBA addition. This phenomenon suggested that $OH^{\cdot}$ did not play an irreplaceable role in the degradation of Rhodamine B, which was consistent with the results of previous studies [51]. There were two C=C double bonds contained in 2,4-HD, which could be easily attacked by peroxyl and acylperoxyl radicals. Therefore, 2,4-HD was used as the quencher for acetyl(per)oxyl radicals [52]. When 100 mmol·L^{-1} 2,4-HD was added, the degradation of Rhodamine B after 60 min decreased from 98.6% to 18.2%. Obviously, acetyl(per)oxyl radicals played the dominant role in the $CuFe_2O_4$/PAA system for the degradation of Rhodamine B. The remaining oxidation capacity of 18.2% was attributed to the existence of $OH^{\cdot}$. MeOH was a strong scavenger for both $OH^{\cdot}$ and organic radicals [1]. When 100 mmol·L^{-1} MeOH was added into the $CuFe_2O_4$/PAA system, the degradation of Rhodamine B after 60 min decreased from 98.6% to 40.2%. According to the above conclusions, acetyl(per)oxyl radicals were the dominant radicals for degradation in the $CuFe_2O_4$/PAA system, whereas $OH^{\cdot}$ played an ancillary role.
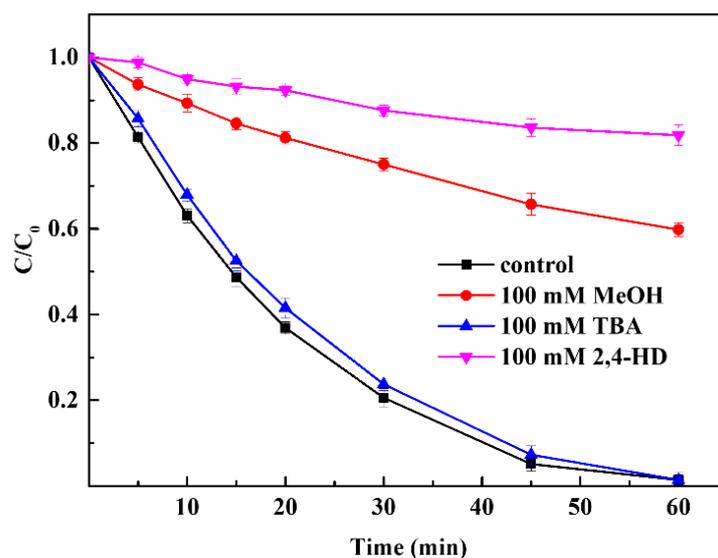

Figure 5. Effect of radical scavengers on Rhodamine B degradation (PAA = 80 mg/L, $CuFe_2O_4$ = 100 mg/L, pH = 7, C_0 = 20 mg/L, room temperature for 1 h).

Based on the above discussion, a possible activation mechanism in $CuFe_2O_4$/PAA was proposed in Figure 6. The degradation of Rhodamine B was attributed to R-O$^{\cdot}$ in the heterogeneous process. During the preliminary stage, $\equiv Cu^{2+}$ accepted an electron from PAA and was converted to $\equiv Cu^+$ which caused the subsequent generation of $CH_3C(O)OO^{\cdot}$. The generated $\equiv Cu^+$ donated an electron to PAA, resulting in the formation of $CH_3C(O)O^{\cdot}$ and the maintenance of the $\equiv Cu^{2+}/\equiv Cu^+$ redox cycle on the surface of the catalyst.

$$\equiv Cu^{2+} + OH^- \rightarrow \equiv CuOH^+ \tag{13}$$
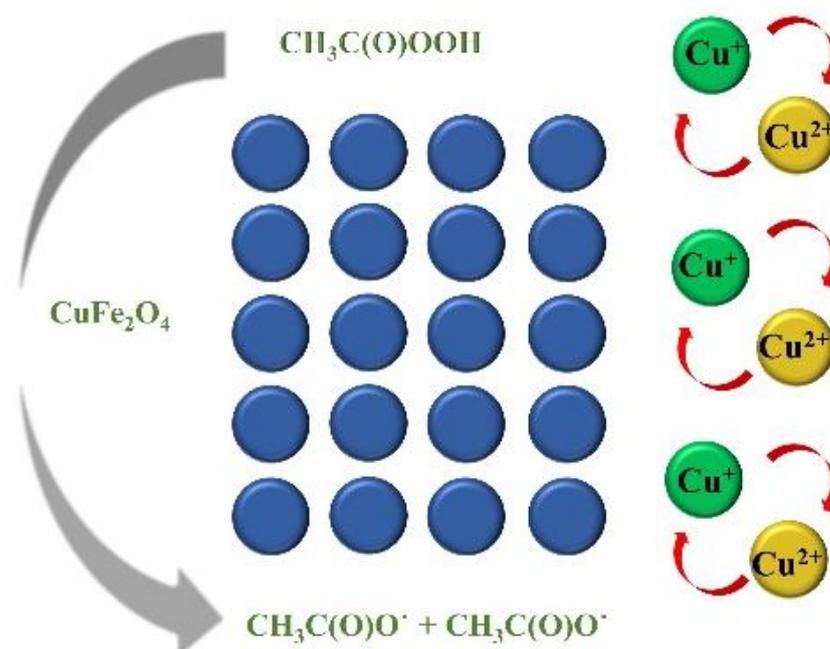
$$\equiv CuOH^+ + OH^- \rightarrow \equiv Cu(OH)_2 \tag{14}$$
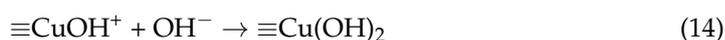
Figure 6. The proposed mechanism of the CuFe$_2$O$_4$/PAA system.

2.6. The Effect of Water Matrices on Contaminant Degradation

Humic acid (HA), Cl$^-$, and HCO$_3^-$ are pervasive substances in natural water which may suppress AOPs [53], so the effect of these naturally occurring anions on the degradation of Rhodamine B was further evaluated. HA could adsorb on the surface of the catalyst and block the catalyst active sites in heterogeneous systems to prevent contact between the oxidant and catalyst [53], resulting in the reduction of catalytic activation efficiency. In addition, R-O· could be partially scavenged by HA, which could also affect the pollutant degradation efficiency. However, the shielding effect was not obvious in the CuFe$_2$O$_4$/PAA system. The effect of HA on Rhodamine B degradation is shown in Figure 7a. Obviously, HA only had a slight impact on Rhodamine B removal in the CuFe$_2$O$_4$/PAA system. As the HA concentration increased from 0 mg/L to 5 mg/L, the removal efficiency after 60 min decreased from 99.2% to 98.7%. This may be because the added CuFe$_2$O$_4$ was in excess for PAA catalysis. In addition, HA may have pro-oxidant properties in AOPs [54]. Moreover, although the generated R-O· could be partially scavenged by HA, as demonstrated in previous studies [18], the remaining R-O· and other radicals such as OH· were abundant enough to lead to Rhodamine B removal.

The effect of HCO$_3^-$ on Rhodamine B degradation is shown in Figure 7b. HCO3$^-$ had an ignorable impact on Rhodamine B removal in the CuFe$_2$O$_4$/PAA system. As the HCO$_3^-$ concentration increased from 0 mmol·L^{-1} to 1 mmol·L^{-1}, the removal efficiency after 60 min decreased from 98.5% to 98.0%. It has been reported that HCO$_3^-$ is a scavenger of hydroxyl radicals and sulfate radicals but could not affect R-O· radicals [22]. Similar to the HA experiment, the disappearance of single free radicals did not affect the overall removal of pollutants. In addition, unreactive carbonate complexes [14,29] were not generated, suggesting the stability of the system. The effect of Cl$^-$ on Rhodamine B removal is shown in Figure 7c. The degradation efficiency of Rhodamine B after 30 min was 76.5%, 72.4%, and 96.2% with 0-, 50-, and 200-mmol·L^{-1} Cl$^-$ added, respectively. The final degradation efficiencies after 60 min were 97.3%, 93.2%, 99.6% with 0, 50, 200 mmol·L^{-1} Cl$^-$ added, respectively. Apparently, the effect of Cl$^-$ on the degradation of Rhodamine B was different under different Cl$^-$ concentrations. A small dosage of Cl$^-$ (10–100 mmol·L^{-1}) suppressed the degradation of Rhodamine B while the addition of 200 mmol·L^{-1} Cl$^-$ promoted the degradation of Rhodamine B. In addition, it was worth noting that the small dosage of Cl$^-$ only slowed down the reaction speed while the final degradation was not seriously

influenced. This was because Cl^- could react with $R\text{-}O^{\cdot}$ and $OH^{\cdot}$ to produce chlorine-containing species that had weaker oxidative capacities [55,56]. When 200 mmol·L^{-1} Cl^- was added, the generation of Cl, $Cl_2^{\cdot}$, and $ClOH^{\cdot}$ compensated for the weakened oxidative capacity, and the radicals even synergized with the remaining $R\text{-}O^{\cdot}$ and $OH^{\cdot}$. In summary, water matrices had only a minimal negative effect on the application of the $CuFe_2O_4$/PAA system, which increased the possibility of the practical application of this type of AOP system.
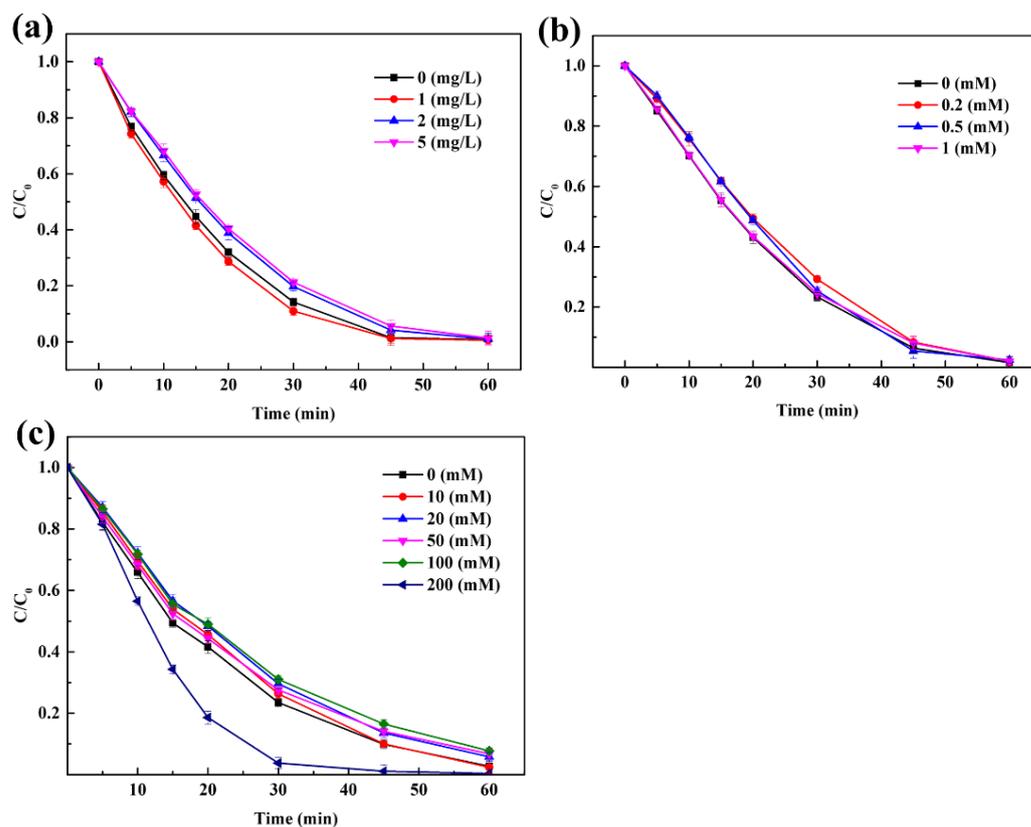

Figure 7. Effect of water matrices. (**a**) HA. (**b**) HCO_3^-. (**c**) Cl^- (PAA = 80 mg/L, $CuFe_2O_4$ = 100 mg/L, pH = 7, C_0 = 20 mg/L, room temperature for 1 h).

2.7. Reusability and Stability of the Catalyst

In terms of practical application, reusability and stability are very important characteristics of a catalyst. To evaluate the reusability of $CuFe_2O_4$, the removal of Rhodamine B by recycling the catalyst after the reaction concluded was conducted under the same experimental conditions ($CuFe_2O_4$ dosage of 100 mg/L, PAA dosage of 80 mg/L, initial pH of 7, and treatment time of 60 min) for four cycles, as shown in Figure 8a. The final removal efficiencies were 98.9%, 89.8%, 99.2%, and 98.2%, respectively, for the four iterative catalyst recycling experiments. It was obvious that $CuFe_2O_4$ demonstrated excellent catalytic performance, and the catalyst maintained a high performance for Rhodamine B decomposition after the fourth iteration of catalyst recycling. Only a 0.7% degradation efficiency decrease was observed, suggesting that $CuFe_2O_4$ possessed high reusability towards PAA activation. In addition, The FTIR spectra of the catalysts before and after the reaction are shown in Figure 8b. No additional functional group characteristic peaks were observed for the recycled $CuFe_2O_4$, illustrating that no passivation occurred on the $CuFe_2O_4$ surface compared with the fresh catalyst, and the catalyst exhibited good catalytic stability. These results suggested that the use of $CuFe_2O_4$ could be operated within a controllable cost window, owing to the high reusability and recyclability of the catalyst.
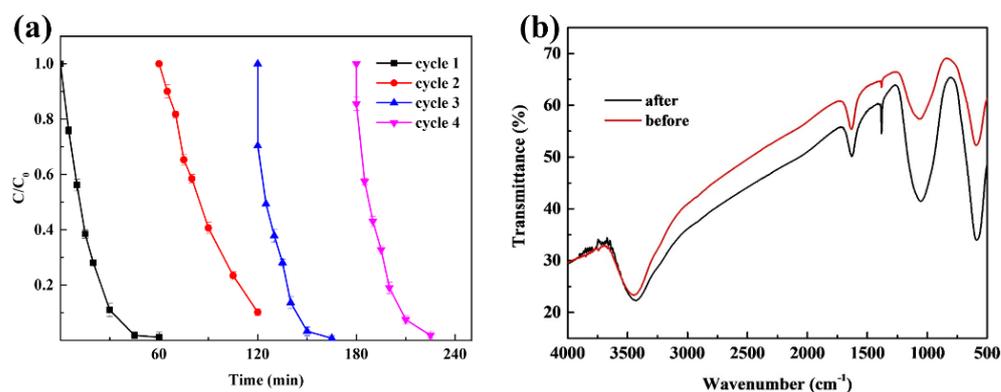
Figure 8. (**a**) Reusability of $CuFe_2O_4$ (PAA = 80 mg/L, $CuFe_2O_4$ = 100 mg/L, pH = 7, C_0 = 20 mg/L, room temperature for 1 h). (**b**) FTIR spectra of $CuFe_2O_4$.

3. Materials and Methods

3.1. Chemicals

Commercial peracetic acid (~20% PAA, ~5% H_2O_2, and ~20% acetic acid; w/w) was obtained from Sigma-Aldrich (St. Louis, MO, USA). $CuFe_2O_4$ with a size of approximately 200 nm was supplied by Aladdin Co., Ltd. (Shanghai, China). Rhodamine B was supplied by Sigma-Aldrich (St. Louis, MO, USA). 2,4-hexadiene (2,4-HD),tert-butyl alcohol (TBA), methanol (MeOH), NaCl, Na_2HCO_3, $Na_2S_2O_3$, and humic acid (HA) were purchased from Aladdin (Shanghai, China). All chemicals were of at least reagent grade and used without further purification. Nano-pure water (resistivity > 18 mΩ cm) was obtained from a Merck Milli-Q Reference system (Darmstadt, Germany).

3.2. Experimental Procedures

Batch degradation experiments were performed at room temperature (25 °C), and the solution was mixed by magnetic stirring in 250 mL amber glass bottles. After an appropriate amount of Rhodamine B solution (20 mg/L) was transferred into the reactor, PAA at designated concentrations (10–100 mg/L) was subsequently added. Then, the initial pH was adjusted by 0.2 mol·L^{-1} NaOH and 0.1 mol·L^{-1} H_2SO_4 solution. The experiments started as soon as the desired amount of $CuFe_2O_4$ was added. The samples were extracted at predetermined time intervals and immediately quenched with excess $Na_2S_2O_3$ (10 mmol·L^{-1}) for the detection of the Rhodamine B concentration. The quenched sample was filtered through a 0.22-μm PTFE membrane, and the filtered sample was subsequently stored at 4 °C before analysis within 24 h.

Cl^- (0–200 mmol·L^{-1}), HCO_3^- (0–1 mmol·L^{-1}), and humic acid (HA, 0–5 mg/L) were added at the beginning of the reaction to evaluate the effect of water matrices on the degradation of Rhodamine B. The same reaction procedures were repeated with tertbutyl alcohol (TBA, 100 mmol·L^{-1}), methanol (MeOH, 100 mmol·L^{-1}), and 2,4-HD (100 mmol·L^{-1}) added at the beginning of the reaction to assess the presence of radical species.

The used $CuFe_2O_4$ was collected via magnetic separation, washed with distilled water, and dried via a vacuum freeze dryer (FD-1A-50, Boyikang, Shanghai, China) to evaluate reusability. All experiments were conducted in duplicate.

3.3. Analytical Methods

N_2 adsorption–desorption measurements were conducted using an ASAP 2020 volumetric adsorption analyzer (Micromeritics, Norcross, GA, USA). The specific surface areas were measured using the standard Brunauer-Emmett-Teller (BET) method. The surface morphology of the samples was characterized via a scanning electron microscope (SEM, ZEISS SUPRA 55, Jena, Germany). The composition and chemical oxidation state of the elements were determined by X-ray photoelectron spectroscopy (XPS, ESCALAB 250Xi, ThermoFisher Scientific, Waltham, MA, USA). Fourier-transform infrared spectroscopy

(FTIR, VERTEX 70, Bruker, Karlsruhe, Germany) was used for the characterization of $CuFe_2O_4$ before and after the reaction. The pH values were measured via a pH meter (Starter-3100, Ohaus, Parsippany-Troy Hills, NJ, USA). The PAA concentration was measured according to the N, N-diethyl-p-phenylenediamine (DPD) colorimetric method [57]. The Rhodamine B concentration was measured via a UV-Vis spectrophotometer (Agilent, Santa Clara, CA, USA) at 553 nm.

4. Conclusions

PAA demonstrated promise as an efficiency disinfectant in AOPs. Spinel ferrite exhibited advantages in terms of structural stability and recovery, and Cu had a lower risk of toxicity and carcinogenicity. The current work demonstrated that the $CuFe_2O_4$/PAA system was a promising process for the degradation of organic pollutants. A pH range of six to eight was suitable for efficient degradation. As the loading of PAA or $CuFe_2O_4$ increased (10–100 mg/L for PAA and 0–100 mg/L for $CuFe_2O_4$), the oxidation of pollutants also increased. Taking into consideration cost control measures and treatment effects, an unlimited increase in dosage was undesirable and unrealistic. When the PAA dose was 80 mg/L and the $CuFe_2O_4$ dose was 100 mg/L, a Rhodamine B removal efficiency of 95.8% was observed, which was sufficient for sewage treatment. PAA activation was dominated by the $\equiv Cu^{2+}/\equiv Cu^{+}$ redox cycle, and the pollutant was removed mainly by the oxidation of $CH_3C(O)O^{\cdot}$ and $CH_3C(O)OO^{\cdot}$. In terms of application in actual wastewater treatment scenarios, a small number of common water matrices (HA, HCO_3^{-}, and Cl^{-}) had a small negative effect on the process, while 200 mg/L of Cl^{-} enhanced the oxidation process. In addition, the $CuFe_2O_4$/PAA system demonstrated satisfying reusability and stability after four recycling iterations. However, further studies are needed in terms of optimization and intensification before promotion and application can be achieved.

Supplementary Materials: The following supporting information can be downloaded at: https://www.mdpi.com/article/10.3390/molecules27196385/s1, Figure S1: Rhodamine B degradation with and without PAA (PAA = 80 mg/L, pH = 7, C_0 = 20 mg/L, room temperature for 1 h), Figure S2: The full scale XPS spectrum of $CuFe_2O_4$.

Author Contributions: F.G. and L.Y. conceived the experiment. C.Y., Y.H. and L.Z. performed the majority of the experiment. F.G., X.Z., Y.Z. and J.C. evaluated and interpreted the data. F.G., C.Y., Y.H. and L.Z. developed the figures. C.Y. wrote the manuscript with participation of all authors. All authors were involved in the discussion and manuscript revision. All authors have read and agreed to the published version of the manuscript.

Institutional Review Board Statement: Not applicable.

Conflicts of Interest: The authors declare no conflict of interest.

Sample Availability: Samples of the Peracetic Acid and $CuFe_2O_4$ are available from the authors.

References

1. Wang, Z.; Wang, J.; Xiong, B.; Bai, F.; Wiesner, M.R. Application of Cobalt/Peracetic Acid to Degrade Sulfamethoxazole at Neutral Condition: Efficiency and Mechanisms. *Environ. Sci. Technol.* **2020**, *54*, 464–475. [CrossRef] [PubMed]
2. Zhou, D.; Chen, L.; Li, J.; Wu, F. Transition Metal Catalyzed Sulfite Auto-oxidation Systems for Oxidative Decontamination in Waters: A state-of-the-art minireview. *Chem. Eng. J.* **2018**, *346*, 726–738. [CrossRef]
3. Xie, P.; Ma, J.; Wei, L.; Jing, Z.; Fang, J. Removal of 2-MIB and geosmin using UV/persulfate: Contributions of hydroxyl and sulfate radicals. *Water Res.* **2015**, *69*, 223–233. [CrossRef] [PubMed]
4. Zhang, W.; Zhou, S.; Sun, J.; Meng, X.; Luo, J.; Zhou, D. Impact of Chloride Ions on UV/H_2O_2 and UV/Persulfate Advanced Oxidation Processes. *Environ. Sci. Technol.* **2018**, *52*, 7380–7389. [CrossRef]
5. Yang, Y.; Pignatello, J.J.; Ma, J.; Mitch, W.A. Effect of matrix components on UV/H_2O_2 and UV/$S_2O_8^{(2-)}$ advanced oxidation processes for trace organic degradation in reverse osmosis brines from municipal wastewater reuse facilities. *Water Res.* **2016**, *89*, 192–200. [CrossRef]
6. Ao, X.; Wang, W.; Sun, W.; Lu, Z.; Li, C. Degradation and transformation of norfloxacin in medium-pressure ultraviolet/peracetic acid process: An investigation of the role of pH. *Water Res.* **2021**, *203*, 117458.

7. Hu, P.D.; Long, M.C. Cobalt-catalyzed sulfate radical-based advanced oxidation: A review on heterogeneous catalysts and applications. *Appl. Catal. B Environ.* **2016**, *181*, 103–117. [CrossRef]

8. Matafonova, G.; Batoev, V. Recent advances in application of UV light-emitting diodes for degrading organic pollutants in water through advanced oxidation processes: A review. *Water Res.* **2018**, *132*, 177–189. [CrossRef]

9. Lu, S.; Wang, N.; Wang, C. Oxidation and biotoxicity assessment of microcystin-LR using different AOPs based on UV, O_3 and H_2O_2. *Front. Environ. Sci. Eng.* **2018**, *12*, 132–138. [CrossRef]

10. Baba, Y.; Yatagai, T.; Harada, T.; Kawase, Y. Hydroxyl radical generation in the photo-Fenton process: Effects of carboxylic acids on iron redox cycling. *Chem. Eng. J.* **2015**, *277*, 229–241. [CrossRef]

11. Zhang, K.; Zhou, X.; Du, P.; Zhang, T.; Cai, M.; Sun, P.; Huang, C.H. Oxidation of beta-lactam antibiotics by peracetic acid: Reaction kinetics, product and pathway evaluation. *Water Res.* **2017**, *123*, 153–161. [CrossRef] [PubMed]

12. Kim, J.; Du, P.; Liu, W.; Luo, C.; Huang, C.H. Cobalt/Peracetic Acid: Advanced Oxidation of Aromatic Organic Compounds by Acetylperoxyl Radical. *Environ. Sci. Technol.* **2020**, *54*, 5268–5278. [CrossRef] [PubMed]

13. Wacawek, S.; Lutze, H.V.; Grübel, K.; Padil, V.; Dionysiou, D.D. Chemistry of persulfates in water and wastewater treatment: A review. *Chem. Eng. J.* **2017**, *330*, 44–62. [CrossRef]

14. Wu, W.; Tian, D.; Liu, T.; Chen, J.; Zhang, Y. Degradation of organic compounds by peracetic acid activated with Co_3O_4: A novel advanced oxidation process and organic radical contribution. *Chem. Eng. J.* **2020**, *394*, 124938. [CrossRef]

15. Silva, W.; Carlos, T.D.; Cavallini, G.S.; Pereira, D.H. Peracetic acid: Structural elucidation for applications in wastewater treatment. *Water Res.* **2020**, *168*, 115143. [CrossRef] [PubMed]

16. Zhou, F.Y.; Lu, C.; Yao, Y.Y. Activated carbon fibers as an effective metal-free catalyst for peracetic acid activation: Implications for the removal of organic pollutants. *Chem. Eng. J.* **2015**, *281*, 953–960. [CrossRef]

17. Kim, J.; Zhang, T.; Liu, W.; Du, P. Advanced Oxidation Process with Peracetic Acid and Fe(II) for Contaminant Degradation. *Environ. Sci. Technol.* **2020**, *53*, 13312–13322. [CrossRef]

18. Chen, S.; Cai, M.Q.; Liu, Y.Z.; Zhang, L.Q. Effects of water matrices on the degradation of naproxen by reactive radicals in the UV/peracetic acid process. *Water Res.* **2019**, *150*, 153–161. [CrossRef]

19. Rizzo, L.; Agovino, T.; Nahim-Granados, S.; Castro-Alferez, M.; Fernandez-Ibanez, P. Tertiary treatment of urban wastewater by solar and UV-C driven advanced oxidation with peracetic acid: Effect on contaminants of emerging concern and antibiotic resistance. *Water Res.* **2019**, *149*, 272–281. [CrossRef]

20. Chen, H.; Lin, T.; Zhang, S.; Xu, H.; Chen, W. Novel FeII/EDDS/UV/PAA advanced oxidation process: Mechanisms and applications for naproxen degradation at neutral pH and low FeII dosage. *Chem. Eng. J.* **2020**, *417*, 127896. [CrossRef]

21. Liu, B.; Guo, W.; Jia, W.; Wang, H. Insights into the oxidation of organic contaminants by Co(II) activated peracetic acid: The overlooked role of high-valent cobalt-oxo species. *Water Res.* **2021**, *201*, 117313. [CrossRef] [PubMed]

22. Cai, M.; Sun, P.; Zhang, L.; Huang, C.H. UV/Peracetic Acid for Degradation of Pharmaceuticals and Reactive Species Evaluation. *Environ. Sci. Technol.* **2017**, *51*, 14217–14224. [CrossRef]

23. Wang, J.; Wan, Y.; Ding, J.; Wang, Z.; Wiesner, M.R. Thermal Activation of Peracetic Acid in Aquatic Solution: The Mechanism and Application to Degrade Sulfamethoxazole. *Environ. Sci. Technol.* **2020**, *54*, 14635–14645. [CrossRef] [PubMed]

24. Sharma, V.K.; Yu, X.; Mcdonald, T.J.; Jinadatha, C.; Dionysiou, D.D.; Feng, M. Elimination of antibiotic resistance genes and control of horizontal transfer risk by UV-based treatment of drinking water: A mini review. *Front. Environ. Sci. Eng.* **2019**, *13*, 9. [CrossRef]

25. Ao, X.W.; Eloranta, J.; Huang, C.H. Peracetic acid-based advanced oxidation processes for decontamination and disinfection of water: A review. *Water Res.* **2020**, *188*, 116479. [CrossRef]

26. Wang, S.; Wang, H.; Liu, Y.; Fu, Y. Effective degradation of sulfamethoxazole with Fe^{2+}-zeolite/peracetic acid—ScienceDirect. *Sep. Purif. Technol.* **2020**, *233*, 115973. [CrossRef]

27. Chen, F.; Zhao, X.; Liu, H.; Qu, J. Reaction of $Cu(CN)_3^{2-}$ with H_2O_2 in water under alkaline conditions: Cyanide oxidation, Cu^+/Cu^{2+} catalysis and H_2O_2 decomposition. *Appl. Catal. B Environ.* **2014**, *158–159*, 85–90. [CrossRef]

28. Ina, E.V.R.; Makarova, K.; Golovina, E.A.; HENK VAN, A.S.; Virkutyte, J. Free Radical Reaction Pathway, Thermochemistry of Peracetic Acid Homolysis, and Its Application for Phenol Degradation: Spectroscopic Study and Quantum Chemistry Calculations. *Environ. Sci. Technol.* **2010**, *44*, 6815–6821.

29. Jw, A.; Bx, A.; Lei, M.A.; Swab, C.; Pxab, D.; Zwab, C.; Jm, E. Applying a novel advanced oxidation process of activated peracetic acid by $CoFe_2O_4$ to efficiently degrade sulfamethoxazole. *Appl. Catal. B Environ.* **2021**, *280*, 119422.

30. Sun, H.; Kwan, C.K.; Suvorova, A.; Ang, H.M.; Tadé, M.; Wang, S. Catalytic oxidation of organic pollutants on pristine and surface nitrogen-modified carbon nanotubes with sulfate radicals. *Appl. Catal. B Environ.* **2014**, *154–155*, 134–141. [CrossRef]

31. Yu, J.; Wang, T.; Rtimi, S. Magnetically separable TiO_2/FeO_x/POM accelerating the photocatalytic removal of the emerging endocrine disruptor: 2,4-dichlorophenol. *Appl. Catal. B Environ.* **2019**, *254*, 66–75. [CrossRef]

32. Karbasi, M.; Karimzadeh, F.; Kiwi, J.; Raeissi, K.; Pulgarin, C.; Rtimi, S. Flower-like magnetized photocatalysts accelerating an emerging pollutant removal under indoor visible light and related phenomena. *J. Photochem. Photobiol. A Chem.* **2019**, *378*, 105–113.

33. Chen, Z.; Wang, L.; Xu, H.; Wen, Q. Efficient heterogeneous activation of peroxymonosulfate by modified $CuFe_2O_4$ for degradation of tetrabromobisphenol A. *Chem. Eng. J.* **2020**, *389*, 124345. [CrossRef]

34. Shih, K.; White, T.; Leckie, J.O. Nickel stabilization efficiency of aluminate and ferrite spinels and their leaching behavior. *Environ. Sci. Technol.* **2006**, *40*, 5520–5526. [CrossRef]

35. Zhang, T.; Zhu, H.; Croué, J. Production of sulfate radical from peroxymonosulfate induced by a magnetically separable CuFe$_2$O$_4$ spinel in water: Efficiency, stability, and mechanism. *Environ. Sci. Technol.* **2013**, *47*, 2784–2791. [CrossRef]

36. Ren, Y.; Lin, L.; Ma, J.; Yang, J.; Feng, J. Sulfate radicals induced from peroxymonosulfate by magnetic ferrospinel MFe$_2$O$_4$ (M = Co, Cu, Mn, and Zn) as heterogeneous catalysts in the water. *Appl. Catal. B Environ.* **2015**, *165*, 572–578. [CrossRef]

37. Yin, X.; Jia, A.; Hui, Z. The mechanism of degradation of bisphenol A using the magnetically separable CuFe$_2$O$_4$/peroxymonosulfate heterogeneous oxidation process. *J. Hazard. Mater.* **2016**, *309*, 87–96.

38. Oh, W.D.; Dong, Z.; Lim, T.T. Generation of sulfate radical through heterogeneous catalysis for organic contaminants removal: Current development, challenges and prospects. *Appl. Catal. B Environ.* **2016**, *194*, 169–201.

39. Zhou, G.; Fu, Y.; Zhou, R.; Zhang, L.; Zhang, L.; Deng, J.; Liu, Y. Efficient degradation of organic contaminants by magnetic cobalt ferrite combined with peracetic acid. *Process Saf. Environ. Prot.* **2022**, *160*, 376–384.

40. Ramos, M.D.N.; Sousa, L.A.; Aguiar, A. Effect of cysteine using Fenton processes on decolorizing different dyes: A kinetic study. *Environ. Technol.* **2020**, *43*, 70–82.

41. Yaseen, M.; Humayun, M.; Khan, A.; Idrees, M.; Shah, N.; Bibi, S. Photo-Assisted Removal of Rhodamine B and Nile Blue Dyes from Water Using CuO-SiO$_2$ Composite. *Molecules* **2007**, *27*, 5343. [CrossRef] [PubMed]

42. Koubek, E.; Haggett, M.L.; Battaglia, C.J.; Ibne-Rasa, K.M.; Edwards, J.O. Kinetics and Mechanism of the Spontaneous Decompositions of Some Peroxoacids, Hydrogen Peroxide and *t*-Butyl Hydroperoxide. *J. Am. Chem. Soc.* **1963**, *85*, 2263–2268.

43. Ghanbari, F.; Giannakis, S.; Lin, K.; Wu, J.; Madihi-Bidgoli, S. Acetaminophen degradation by a synergistic peracetic acid/UVC-LED/Fe(II) advanced oxidation process: Kinetic assessment, process feasibility and mechanistic considerations. *Chemosphere* **2020**, *263*, 128119.

44. Georgi, A.; Schierz, A.; Trommler, U.; Horwitz, C.P.; Collins, T.J.; Kopinke, F.D. Humic acid modified Fenton reagent for enhancement of the working pH range. *Appl. Catal. B Environ.* **2007**, *72*, 26–36.

45. Bai, R.; Yan, W.; Xiao, Y.; Wang, S.; Tian, X. Acceleration of peroxymonosulfate decomposition by a magnetic MoS$_2$/CuFe$_2$O$_4$ heterogeneous catalyst for rapid degradation of fluoxetine. *Chem. Eng. J.* **2020**, *397*, 125501.

46. Zhang, H.; Li, C.; Lai, L.; Hu, C. Surface oxygen vacancy inducing peroxymonosulfate activation through electron donation of pollutants over cobalt-zinc ferrite for water purification. *Appl. Catal. B Environ.* **2020**, *270*, 118874. [CrossRef]

47. Liu, Z.; Yang, S.; Yuan, Y.; Xu, J.; Zhu, Y.; Li, J.; Wu, F. A novel heterogeneous system for sulfate radical generation through sulfite activation on a CoFe$_2$O$_4$ nanocatalyst surface. *J. Hazard. Mater.* **2016**, *324*, 583–592.

48. Yao, Y.; Lu, F.; Zhu, Y.; Wei, F.; Liu, X.; Lian, C.; Wang, S. Magnetic core–shell CuFe$_2$O$_4$@C$_3$N$_4$ hybrids for visible light photocatalysis of Orange II. *J. Hazard. Mater.* **2015**, *297*, 224–233. [CrossRef]

49. Chu, W.; Xu, B. Ozonation of phenacetin in associated with a magnetic catalyst CuFe$_2$O$_4$: The reaction and transformation. *Chem. Eng. J.* **2015**, *262*, 552–562.

50. Anipsitakis, G.P.; Dionysiou, D.D. Radical Generation by the Interaction of Transition Metals with Common Oxidants. *Environ. Sci. Technol.* **2004**, *38*, 3705–3712.

51. Yan, J.F.; Li, J.; Peng, J.L. Efficient degradation of sulfamethoxazole by the CuO@Al$_2$O$_3$ (EPC) coupled PMS system: Optimization, degradation pathways and toxicity evaluation—ScienceDirect. *Chem. Eng. J.* **2019**, *359*, 1097–1110. [CrossRef]

52. Chateauneuf, J.; Lusztyk, J.; Ingold, K.U. Spectroscopic and kinetic characteristics of aroyloxyl radicals. 1. The 4-methoxybenzoyloxyl radical. *J. Am. Chem. Soc.* **1988**, *110*, 2877–2885. [CrossRef]

53. Bennedsen, L.R.; Muff, J.; Sogaard, E.G. Influence of chloride and carbonates on the reactivity of activated persulfate. *Chemosphere* **2012**, *86*, 1092–1097. [CrossRef]

54. García-Ballesteros, S.; García-Negueroles, P.; Amat, A.M.; Arques, A. Humic-Like Substances as Auxiliaries to Enhance Advanced Oxidation Processes. *ACS Omega* **2022**, *7*, 3151–3157. [CrossRef]

55. Shah, A.D.; Liu, Z.Q.; Salhi, E.; Hoefer, T.; Gunten, U.V. Peracetic Acid Oxidation of Saline Waters in the Absence and Presence of H$_2$O$_2$: Secondary Oxidant and Disinfection Byproduct Formation. *Environ. Sci. Technol.* **2015**, *49*, 1698–1705. [CrossRef]

56. Bojing, S.; Wenjie, W.; Leijiang, Z.; Honghong, Z. Polyaniline: A New Metal-Free Catalyst for Peroxymonosulfate Activation with Highly Efficient and Durable Removal of Organic Pollutants. *Environ. Sci. Technol.* **2019**, *53*, 9771–9780.

57. Masini, J.C.; Abate, G.; Lima, E.C.; Hahn, L.C.; Nakamura, M.S.; Lichtig, J.; Nagatomy, H.R. Comparison of methodologies for determination of carboxylic and phenolic groups in humic acids. *Anal. Chim. Acta* **1998**, *364*, 223–233. [CrossRef]